Lab on a Chip

Cite this: *Lab Chip*, 2011, **11**, 3855

www.rsc.org/loc

PAPER

Dynamic measurement of the height and volume of migrating cells by a novel fluorescence microscopy technique

Céline Bottier,†*[a] Chiara Gabella,†[a] Benoît Vianay,[a] Lara Buscemi,[a] Ivo F. Sbalzarini,[b] Jean-Jacques Meister[a] and Alexander B. Verkhovsky[a]

Received 25th August 2011, Accepted 8th September 2011
DOI: 10.1039/c1lc20807a

We propose a new technique to measure the volume of adherent migrating cells. The method is based on a negative staining where a fluorescent, non-cell-permeant dye is added to the extracellular medium. The specimen is observed with a conventional fluorescence microscope in a chamber of uniform height. Given that the fluorescence signal depends on the thickness of the emitting layer, the objects excluding the fluorescent dye (*i.e.*, cells) appear dark, and the decrease of the fluorescent signal with respect to the background is expected to give information about the height and the volume of the object. Using a glass microfabricated pattern with steps of defined heights, we show that the drop in fluorescence intensity is indeed proportional to the height of the step and obtain calibration curves relating fluorescence intensity to height. The technique, termed the fluorescence displacement method, is further validated by comparing our measurements with the ones obtained by atomic force microscopy (AFM). We apply our method to measure the real-time volume dynamics of migrating fish epidermal keratocytes subjected to osmotic stress. The fluorescence displacement technique allows fast and precise monitoring of cell height and volume, thus providing a valuable tool for characterizing the three-dimensional behaviour of migrating cells.

Introduction

Cell volume regulation is essential for many cellular functions including transepithelial transport, metabolism, excitation, hormone release, cell proliferation, and cell death.[1] Both cell swelling and shrinkage serve as signals for initiating or modulating different biochemical reactions in eukaryotic cells.[2] In particular, water channels have been suggested to play a fundamental role in cell migration,[3] and they may thus be important for various biological phenomena such as wound healing, tumour spread, and organ regeneration. Interestingly, osmotic stress was reported to have different effects on migration, depending on cell types. For instance, the migration of leukocytes was strongly inhibited by hypertonic stress and stimulated by hypotonic stress,[4,5] while the migration of transformed renal epithelial cells was inhibited by both hypo- and hypertonicity.[6]

The plasma membrane of most cells that endure osmotic stress undergoes changes in tension.[1,7] The balance between membrane tension and actin assembly may play an important role in controlling the cell shape and migration velocity.[8–11] The two-dimensional cell shape was linked to migration mechanisms in different models.[9,12] The motion of the bulk of the cytoplasm and cytoplasmic flows were also suggested to play an important role in the migration mechanism,[13–15] but the three-dimensional dynamics of cell height and volume during migration is largely unknown. This gap in our knowledge is in a significant part due to the fact that most of the methods proposed so far to measure cell height profiles and volumes are not well suited for adherent migrating cells and/or require sophisticated and dedicated equipment that is not easily compatible with conventional live-cell microscopy.

Several methods have been developed for measuring cell volume. Assuming spherical cells, the Coulter counting technique[16,17] (impedance measurement) and conventional light microscopy[18] are commonly used for measuring the volume of cells in suspension. Light microscopy was also used for estimating the volume of adherent cells based on their attachment area,[19] but this requires assuming a constant cell thickness, which is rarely the case. The volume of adherent cells was also estimated by counting interference fringes in interference reflection microscopy images.[20] The number of fringes between a site in the cell and the cell edge gives information about the height at this site; however, the fringes may result from depression as well as elevation, and in the case of a steep height gradient they may be difficult to resolve. Boudreault and Grygorczyk developed

[a]*Ecole Polytechnique Fédérale de Lausanne, Laboratory of Cell Biophysics, Station 19, CH-1015 Lausanne, Switzerland. E-mail: celine.bottier@epfl.ch until end of 2011, then: celine.bottier@cirad.fr; Fax: +41-21-693-83-05; Tel: +41-21-693-83-49*
[b]*ETH Zurich, Institute of Theoretical Computer Science and Swiss Institute of Bioinformatics, Universitätstr. 6, CH-8092 Zurich, Switzerland*
† These authors contributed equally to this paper.

a method using conventional microscopy where a glass substrate is mounted vertically in the chamber providing a side view of the cells.[21] With such a setup it was, however, difficult to simultaneously obtain also the top view of the cell, rendering it inappropriate for the observation of rapidly migrating cells.

The volume of adherent cells can also be determined using techniques of scanning probe microscopy. Among these, atomic force microscopy (AFM) offers a very high spatial resolution;[22] however, scanning a whole cell requires significant time, which could pose problems with rapidly moving cells. Using scanning ion conductance microscopy, it is possible to determine a large range of volumes (from 10^{-19} to 10^{-9} litres) with a very high resolution of 2.5×10^{-20} litre,[23] but this method, as AFM, requires sophisticated and dedicated equipment.

Several techniques are based on the use of fluorescent markers. In one approach, cells are loaded with a dye and volume changes are related to the intensity of the fluorescence signal. Cell swelling implies a dilution of the dye (*i.e.*, a decrease of the fluorescence intensity) whereas shrinkage concentrates the marker inside the cell.[24] This method detects relative volume changes; however, the determination of the absolute volume requires separate three-dimensional reconstruction from confocal images. Additionally, introducing fluorescent molecules into the cytoplasm may affect and/or modify cell properties. Attaching fluorescent particles to the cell surface and tracking their position over time were used to measure cell height changes without compromising the integrity of the cell;[25] however, the information is limited to the sites of bead attachment and the presence of a halo around the particles renders the precise determination of their positions difficult.

Recently, a few studies presented approaches based on negative staining. In these techniques, a membrane-impermeant dye is added to the extracellular medium and the cell volume is evaluated as the space containing no dye. The group of Model used a strongly absorbing dye in combination with transmission microscopy.[26,27] This setup produced high-contrast images where the cells appeared brighter than the background due to the lack of absorbing dye in the cell volume. Exchangeable filters had to be used in the transmission light path to combine this method with other modes of microscopy. A more important limitation is that absorbing dyes were used in a very high concentration, which entails the risk of toxicity and photodamage to the cell. In order to increase the resolution of the method, it was proposed to work with fixed cells using even higher concentrations of dyes.[28] Wide availability and high efficiency of fluorescent dyes make it very attractive to try using conventional fluorescence microscopy for negative staining, whereby one could expect to achieve sufficient contrast with much lower dye concentration. Indeed, Droste *et al.* used a fluorescent dye in combination with confocal laser scanning microscopy (CLSM).[29] The main limitations of their technique are the extended recording time (50 to 60 seconds) required to acquire the raw data of a single isosurface, and the limited vertical resolution of confocal microscopy rendering the detection of thin cell structures such as lamellipodia[30] problematic. Moreover, three-dimensional reconstruction from confocal sections is a complex task. These issues make it difficult to apply this method for volume imaging of rapidly migrating cells. Using wide-field fluorescence microscopy instead of confocal microscopy could have solved these issues. However, in wide-field microscopy, the signal is collected from the whole depth of the sample, and one would first have to demonstrate that a slight difference in fluorescence intensity due to the exclusion of dye from the cell volume is detectable over the bright fluorescent background, and that it can be related to cell height.

Here, we present a novel application of the negative staining concept to measure cell height and volume using conventional fluorescent dyes and a conventional wide-field fluorescence microscopy setup. We demonstrate that thin cell structures provide sufficient contrast over a much thicker layer of fluorescent solution, that the loss of fluorescence signal is proportional to the cell height, and that the loss of signal is insensitive to the focus position. We calibrate our method using etched glass patterns of known heights and further validate it by performing real-time height and volume measurements in a well-established model system for cell migration, fish epidermal keratocytes.[31] Fish keratocytes are remarkable for their stable shape and fast, persistent migration. After polarization, keratocytes adopt a "canoe" shape viewed from the top, whereas viewed from the side they display a "fried-egg" profile with a flat lamellipodium in the front and a round cell body trailing behind.[30] In these cells, the local thickness varies greatly between the lamellipodium (~100 to 200 nm)[32] and the body (~4 to 8 μm),[20,32,33] making them a good test object for vertical profile measurements. We show that measurements of the cell height profile and volume by the present fluorescence displacement method agree well with results from AFM. We then demonstrate the use of our method in an exemplary application to characterize the volume and vertical profile changes in migrating keratocytes under osmotic stress.

Materials and methods

Cell culture

Black tetra (*Gymnocorymbus ternetzi*) epidermal keratocytes were cultured in Dulbecco's Modified Eagle Medium (DMEM) supplemented with 10% fetal bovine serum and antibiotics, as previously described.[34] Briefly, the fish scales were extracted with tweezers, placed on a 24×60 mm^2 dry glass coverslip (MenzelGläser, Germany), and allowed to adhere for 30 to 60 seconds to prevent them from floating. The culture medium was then added and the keratocytes were allowed to migrate to form colonies on the coverslips overnight at 30 °C. To obtain free locomoting keratocytes, the cell colonies were treated for 3 minutes with 0.25% trypsin–EDTA solution (Sigma-Aldrich, USA) and rinsed with culture medium. They were allowed to separate from the colonies and migrate individually for 30 minutes before assembling the coverslip into the observation chamber.

NIH 3T3 fibroblasts were cultured in DMEM supplemented with 10% fetal bovine serum and antibiotics and were harvested with trypsin–EDTA solution (Sigma-Aldrich, USA). Cells were plated on 24×60 mm^2 glass coverslips and left to spread for two days before the AFM experiment.

Preparation of the observation chambers and perfusion solutions

Two types of observation chambers were used. To get detailed images of thin cell structures (*i.e.* lamellipodium), we used a very thin custom chamber (~15 μm height). It was built by putting

a glass coverslip (22 × 22 mm^2) on top of the coverslip with cells (24 × 60 mm^2). As a spacer between these two coverslips, we used very thin adhesive double tape ("Glue-it Permanent" Compact Roller, Pritt, Germany). Based on the contact area between the coverslips (~2 cm^2 excluding the tape area) and the volume of liquid in the chamber (~3 μL), we estimated the height of the chamber at approximately 15 μm. Vacuum grease (DC4 electrical compound, Dow Corning, USA) can also be used to obtain similar chamber height.

The second type of chamber was used for long-term observation during osmotic treatment of the cells. To facilitate the exchanges of solutions in these experiments, we used a commercially available sticky microfluidic channel (Ibidi, Germany). The chamber was built by simply sticking the channel (100 μm height + maximum 50 μm for the sticky layer) to the coverslip (24 × 60 mm^2), on which the cells were cultured.

Osmolality measurements were performed using the freezing point depression method (Fiske 210 micro-sample osmometer, Advanced Instruments, USA). Culture medium containing 25 μM rhodamine B isothiocyanate-dextran (M_W = 10 000 g mol^{-1}, Sigma-Aldrich, USA) was used as isotonic solution (osmolality 240 mOsm kg^{-1} H_2O). For osmotic treatments, we used a hypotonic shock solution obtained by diluting the cell culture medium with an equal volume of deionized water while keeping the dye concentration constant at 25 μM (osmolality 120 mOsm kg^{-1} H_2O). Applying osmotic transitions from isotonic to hypotonic and from hypotonic to isotonic solutions allows investigating cell swelling and shrinkage responses, respectively. To change the solutions in the microfluidic channel, the solution was introduced from the inlet of the channel using a pipette while the content of the channel was simultaneously aspirated from the outlet using a filter paper. Introducing a large volume of new solution (~200 μL) compared to the volume of the channel (25 μL) ensures a complete change of solutions in the microfluidic channel.

Imaging techniques for volume measurements

Fluorescence and phase-contrast microscopy were performed on an inverted microscope (Eclipse TE300, Nikon, Japan) using different objective lenses (Nikon Plan Fluor, 40×, NA 0.75 Air; Nikon Plan, 40×, NA 1.0 Oil; Nikon Plan, 100×, NA 1.25 Oil) and cooled charge-coupled device cameras (Micromax 1024BFT; Roper Industries, USA; CoolSNAP HQ2, Photometrics, USA) operated with MetaMorph software (Universal Imaging, USA). Fluorescence image sequences in the rhodamine channel were obtained using time interval between frames varying from 5 to 60 seconds and exposure times of 30–200 ms. Exposure time was chosen to obtain a background fluorescent intensity of approximately 60–80% of the camera saturation level which ensured the linearity and sensitivity of the signal detection. We used a high magnification lens (100×) to get details of cell morphology during swelling or shrinkage and a low magnification lens (40×) to record long volume dynamics.

Despite careful alignment of the excitation source (100 W HBO lamp), a gradient of intensity was detected in the illumination field between the centre and the corners of the image. To attenuate this gradient, each recorded image was divided by the background image (recorded from the field containing no cells) and then multiplied by the mean intensity of the background image. This procedure renders the background homogeneous on the entire image and improves the detection of very thin and flat structures (*i.e.* lamellipodium). A low-pass filter with width and height of 5 pixels was subsequently applied to diminish the noise.

Atomic force microscopy (AFM)

Surface topography images of living cells were obtained using a Nanowizard II AFM (JPK Instruments, Germany) in contact mode. We used silicon nitride cantilevers (Microlevers, Veeco Instruments) with nominal spring constants of 0.06 N m^{-1}. The height profiles were obtained using the JPK Image Processing software (JPK Instruments, Germany).

Depending on the cell type (keratocyte or fibroblast), different imaging conditions were applied. Because of the rapid motion of keratocytes (~10 to 15 μm min^{-1}), we used a rapid scan rate of 2 Hz and a low resolution (64 pixels) so that an image could be acquired in less than 40 seconds. The slowly moving 3T3 fibroblasts were imaged using a slow scan rate of 0.5 Hz and a higher resolution (256 pixels), resulting in an acquisition time of 10 minutes. After AFM imaging, the coverslip with the fibroblasts was assembled with the microfluidic channel for the fluorescence measurement and transferred to the inverted microscope. To localize the same cell that was imaged with AFM, we generated marks on the coverslip by scratching it with a piece of silicon wafer. To compare the AFM and fluorescence images, they were superimposed using Photoshop (Adobe) and colour-coded in the same way using a custom-made Matlab (MathWorks, USA) script.

Microfabrication of the calibration sample and calibration procedure

To obtain a relation between the fluorescence intensity and the height of the object displacing the fluorescent medium, we measured the fluorescence of dextran solution loaded between a coverslip and a fabricated glass substrate etched with a controlled depth. This substrate, termed calibration sample below, was fabricated from a Pyrex wafer (22 × 22 mm^2, Sensor Prep. Services, USA). This material was chosen for its non-reflectivity to avoid parasitic reflexions, which would disturb the fluorescence measurement. Pyrex is also well suited for microelectronics procedures, which were performed at the Center of MicroNanoTechnology at EPFL.

Two successive photolithographies, each followed by a wet etching, were performed to create the three-dimensional surface. The photolithography process consisted of a coating with a 2 μm layer of photoresist (AZ 1512; Microchemicals, Germany), a UV exposure through a chrome mask, followed by a development (MIF 726, Microchemicals, Germany) that removed the exposed photoresist layer. The wet etching of the Pyrex was done using buffered hydrofluoric acid (7 : 1, Microchemicals, Germany). Using an etching speed of 30 nm min^{-1}, a first step of 460 nm depth was created. During the second photolithography, the position of the chrome mask was slightly shifted and a different etching time was used so that previously non-exposed regions were etched at 630 nm and previously exposed regions at 1090 nm. The heights of those three steps were controlled with a profilometer (Alpha-Step 500, Tencor, USA).

To prepare the calibration chamber in a way similar to the observation chambers, we used a spacer between the glass coverslip (24 × 60 mm^2) and the calibration sample (positioned etched side towards the coverslip). As we used two types of observation chambers (a custom thin chamber and a microfluidic channel), we also performed the calibration using two types of spacers. In one case, the calibration chamber was prepared in exactly the same way as the custom chamber by using adhesive double tape as a thin spacer (15 μm). In the other case, the Ibidi channel was emulated by using coverslips (130–160 μm height range) at two sides of the chamber as a thick spacer. The height of a coverslip is roughly equivalent to the height of the Ibidi channel of 100 μm + maximum 50 μm for the sticky layer, as given by the manufacturer.

The calibration chambers were filled with culture medium containing the fluorescent dye. Since the calibration sample was not sufficiently optically clear to be imaged through it, the chamber was positioned coverslip-side towards the objective lens and the calibration sample on top of it with a spacer in-between. Using phase-contrast microscopy, the lens was focused on a region of interest (*i.e.*, presenting the three different etched depths as well as the non-etched region in the same field of view) and a fluorescence picture was then acquired (see Fig. 2A). The intensity levels (I) were measured in each region; the intensity of the non-etched region (I_0) was subtracted from the intensities of each of the etched regions and the values $I-I_0$ were plotted as a function of the height difference (ΔH) (see Fig. 2B and E). The slope of this calibration curve gave the coefficient for the conversion of fluorescence intensity to height. Error bars were obtained from 10 measurements that were done by assembling and disassembling the chamber for each measurement. Each measurement represents the mean intensity level of an area of approximately 200 and 30 μm^2 for 40× and 100× lenses, respectively.

The orientation of the calibration chamber implies that emission light passes through a layer of dye solution before reaching the calibration sample, which, in the case of a thick spacer, could result in attenuation of the emission light due to absorption. To avoid this potential problem, we used lower dye concentration (5 instead of 25 μM) when working with thick spacer. To compare the intensities measured with thin (undiluted dye) and thick (diluted dye) spacers, we multiplied the latter values by the dilution factor. Note that the absorption was not expected to be a problem during cell volume measurement because, as opposed to the calibration sample, the coverslip with cells was positioned next to the objective lens. Consequently, the measured difference in the intensity between the cell and the background was due to the emission from the solution layer that was closest to the excitation source and thus received non-attenuated light.

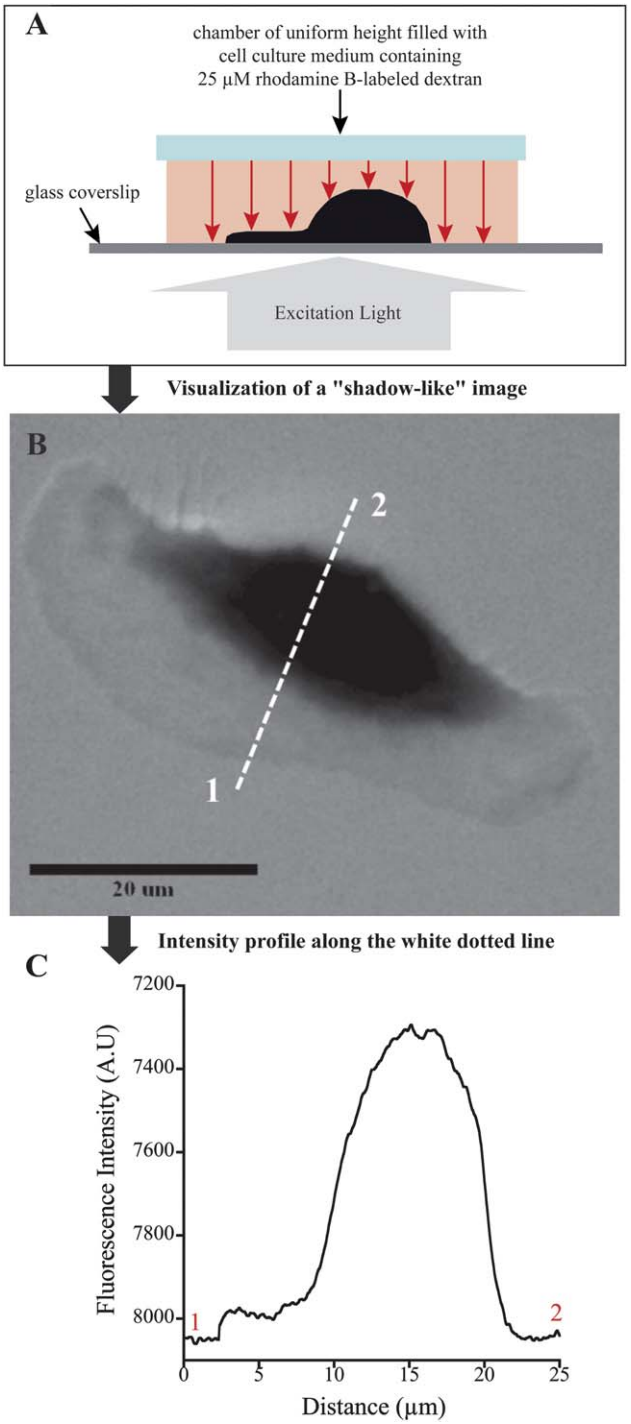

Fig. 1 Principle of the fluorescence displacement method for volume measurement. (A) Schematic view of the setup made of a chamber of uniform height containing a migrating cell (not drawn to scale). The chamber is filled with medium containing a fluorescent dye and illuminated with an epifluorescence setup. (B) Fluorescence image of a migrating fish epidermal keratocyte (observed with a 100× lens). This setup generates "shadow-like" images where the decrease in fluorescence intensity is related to the cell height. (C) Fluorescence intensity profile (shown inverted) along the white dotted line in (B), where the lamellipodium (distances between ~2.5 and 8 μm) and the cell body (distances between ~8 and 23 μm) can be identified. Bar: 20 μm.

Results and discussion

Principle of the volume measurement technique

The present method, termed the fluorescence displacement technique, is based on measuring the emitted intensity from a layer of solution containing a fluorescent dye. When the dye is illuminated at its excitation wavelength, the intensity of the collected light is proportional to the number of excited

molecules. We used wide-field fluorescence microscopy where the emitted light is collected from the whole volume, meaning that the number of excited molecules and thus the intensity should be proportional to the thickness of the emitting layer, provided the dye is homogeneously distributed in the solution. If a non-fluorescent transparent object displaces the solution, the thickness of the emitting layer would be reduced and the fluorescence intensity is expected to decrease. In a chamber of uniform height providing uniform background, it should hence be possible to relate the decrease in fluorescence intensity with respect to the background to the height of the displacing object. However, it was necessary to test if the decrease of fluorescence intensity due to the displacement by thin cell structures such as lamellipodium could be in fact observed and measured.

The principle and feasibility of the method are illustrated in Fig. 1. Panel A displays the diagram of the setup (also see Methods) and panel B shows an image of fish epidermal keratocyte obtained with this setup. Remarkably, we could indeed observe a "shadow-like" image of the cell with the thicker cell body appearing darker than the thin lamellipodium. The fluorescence intensity profile (Fig. 1C) was consistent with previous AFM[33] and electron microscopy[30] data about the height profile of migrating keratocytes.

We checked the non-toxicity of the fluorescent marker by incubating the cells with the dye for several hours. We did not notice any changes in the migratory behaviour of the cells. We also verified that there was no significant penetration of the dextran into the keratocytes over a period of a few hours (data not shown). Note that other fluorescent dyes can be used for other types of cells if any adverse effects or interactions with dextran are observed.

Linearity and calibration of the height measurement

To establish a relationship between fluorescence intensity and the height of the object displacing the fluorescent solution we used a calibration sample made of a Pyrex substrate etched at different depths: 460, 630, and 1100 nm. These values are in a similar range to the structures we expect to detect: the lamellipodium (~100 to 200 nm) and the cell body (~several μm).

The etched steps were clearly identifiable by their different intensities in the fluorescence image of the calibration sample filled with dye-containing culture medium (Fig. 2A). We subtracted the intensity of the non-etched region from the intensities of etched regions and plotted the resulting intensity differences as a function of the etching depth (Fig. 2B and E). The intensity changed linearly with etching depth, demonstrating the proportionality between the thickness of the emitting layer and the fluorescence intensity. This linear relationship was observed for lenses of different magnifications, air as well as oil-immersion (we tested 40× oil and air and 100× oil; the calibrations for the latter two are presented in Fig. 2B and E). The slope of the line is the coefficient of proportionality between intensity and height, which we subsequently used to determine the cell height.

Since chambers of different thickness were used for cell imaging (see below), we also tested if the thickness of the dye solution layer affects the linearity and the calibration slope. To control the dye solution thickness, we used two spacer sizes: adhesive tape of ~15 μm and a coverslip of 130–160 μm (see Materials and methods).

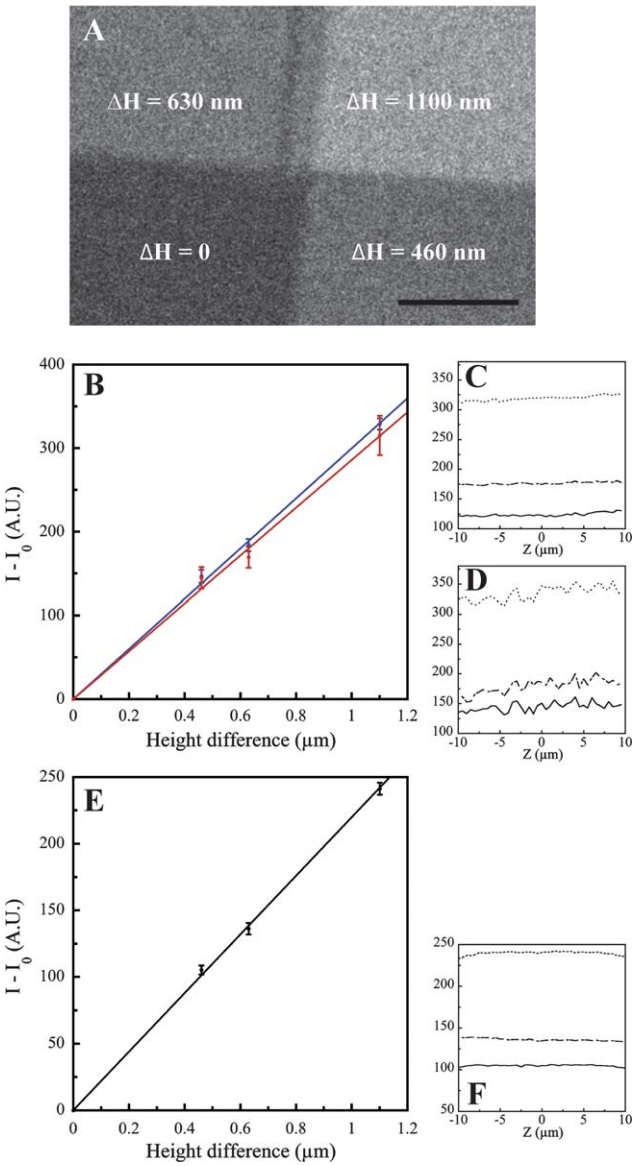

Fig. 2 Linear relationship between cell height and fluorescence intensity. (A) Fluorescence image (acquired with a 40× lens) of the calibration sample filled with dye-containing culture medium showing different regions etched into the glass with different depths (460, 630, and 1100 nm). The intensity of the non-etched region (I_0) is subtracted from the measured intensities (I) of the other regions. (B) Plot of the $I - I_0$ values *vs.* etching depth. Measurements were performed with the 40× lens using a thin (blue line) and a thick (red line) spacer inserted between the bottom coverslip and the calibration sample. (C) and (D) show the variations of $I - I_0$ when varying the focus of the microscope with the 40× lens using a thin and a thick spacer, respectively. Measurements were performed on the three different regions: $H = 460$ nm (solid line), $H = 630$ nm (dashed–dotted line), and $H = 1100$ nm (dotted line). (E) Plot of the $I - I_0$ values *vs.* etching depth with the 100× lens and a thin spacer. (F) shows the variations of $I - I_0$ when varying the focus of the microscope with the 100× lens and a thin spacer. Symbols as in (C) and (D). Bar: 50 μm.

Fig. 2B shows that the calibration slopes obtained using a thin (blue line) and a thick spacer (red line) were nearly identical, although the measurements with the thick spacer displayed a higher dispersion (see error bars). We conclude that the detection of submicrometre structures is possible even over a bright

fluorescent background due to the solution layer of over 100 μm thickness. Moreover, the linear relationship between the fluorescent intensity difference and the height of the structures is not affected by the overall height of the chamber. However, using a thick chamber results in a deterioration of the signal-to-noise ratio of the measurement. This is because the background fluorescence intensity has to be kept within the dynamic range of the camera. Consequently, increasing the chamber thickness requires either the dilution of the dye or the decrease of exposure time, which reduces the signal from thin features. This effect was evident as increasing dispersion of the calibration measurement. Based on the standard deviations of the measurements, we could expect up to 10% error in the determination of the calibration slope when using a thick chamber.

We noticed that the calibration slope was sensitive to the alignment of the excitation source, which could not always be precisely controlled. To decrease the experimental error stemming from this factor, we performed a calibration immediately before each experimental run and we used the corresponding slope to translate the intensities to heights.

An additional point to be addressed was whether the measurements were affected by the position of the microscope's focal plane. As a rule, we used phase-contrast images to position the focal plane at the cell/substrate interface; however, changing solutions in the perfusion chamber may result in transient changes of the focus. Additionally, parts of the cell, such as the cell body, may be relatively high over the substrate and hence far from the microscope's focal plane. Therefore, it was important to test if the contribution from out-of-focus objects to the reduction of fluorescence intensity was comparable to the contribution from in-focus objects. To address this, we imaged the calibration sample with varying focus positions in the range of −10 to +10 μm with respect to the substrate plane using a piezoelectric device. Fig. 2C, D and F show the focus variation measurements for the 40× lens in a chamber with a thin spacer, 40× lens with a thick spacer and 100× lens with a thin spacer, respectively. As noted above, using a thick spacer significantly increases the noise of the measurement (Fig. 2D). Steep boundaries between the regions of different depth appeared blurred when out of focus; nevertheless, the intensity differences between the regions were not significantly affected by the focal position, indicating that height and volume could be reliably measured even for far out-of-focus objects. Note, however, that defocusing could result in flattening of the steep height profiles, because out-of-focus features with high relief (such as steps of the calibration sample) will be blurred in fluorescence displacement images.

Validation of the technique by AFM

In order to further validate the fluorescence displacement technique, we used the above calibration curves to obtain cell height

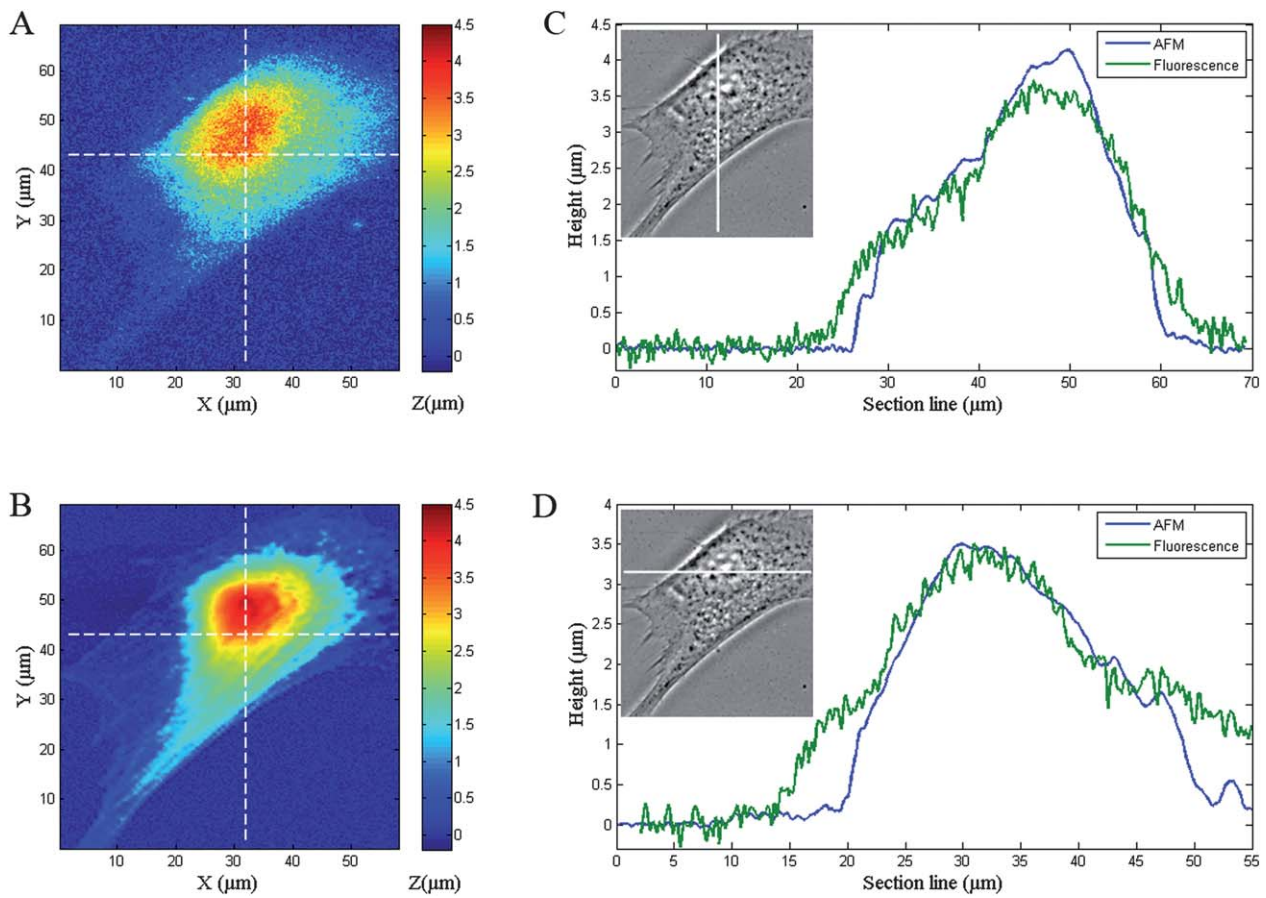

Fig. 3 Comparison of the fluorescence displacement technique with AFM. The height maps of a fibroblast were measured using the fluorescence displacement technique (A) and atomic force microscopy (B) and coded with the same colour scale. (C) and (D) show the height profiles obtained with AFM (blue lines) and the fluorescence displacement technique (green lines) along the white lines indicated on phase-contrast images in the insets.

maps and compared the results with the ones obtained with AFM. Note that, even with the fast AFM scan (about 40 seconds, see Materials and methods), it is impossible to measure the volume of living migrating keratocytes because the cell moves about half its size during the time of the scan. This is why we have chosen the maximum cell height as a parameter to compare our method to AFM. We measured the maximal height of the cell body (H_{max}) by plotting the height profile in the direction of cell motion through the middle of the cell. Measuring two independent populations of migrating keratocytes with both AFM and the fluorescence displacement technique yielded similar results: $H_{max} = 3.65 \pm 0.86$ μm ($N = 30$ cells) with the fluorescence displacement technique and $H_{max} = 3.70 \pm 0.69$ μm ($N = 22$ cells) with AFM. The volumes of the same population of keratocytes measured by the fluorescence displacement technique showed a broad variation from approximately 300 to 1200 μm^3 (mean = 730 ± 200 μm^3, $N = 26$ cells). As mentioned above, it was impossible to measure the volume of living keratocytes with our AFM setup but the measurement of the volumes of fixed cells gave a comparable value: $V = 860 \pm 260$ μm^3 ($N = 7$ cells).

To image the same living cell by our method and AFM, we used slowly moving 3T3 fibroblasts (Fig. 3). Fig. 3 shows height maps (A and B) and profiles (C and D) obtained by the two methods. Despite the higher resolution of AFM compared to fluorescence imaging, a rather good superposition of the profiles obtained by both techniques was observed. Note that imperfect match between the profiles could be the result of cell motion and change of shape during the time of transfer between the AFM and fluorescence microscope. Also, a lower resolution of the fluorescence method compared to AFM and some blurring of steep out-of-focus features (see the previous section) could result in a flattened profile. Integrating the height maps obtained by the two methods gave similar values for the volume of the cell: 2060 μm^3 by AFM and 2210 μm^3 by the fluorescence displacement method.

Volume response of migrating cells to osmotic stress

The fluorescence displacement technique was applied to investigate the volume response of a single migrating cell under osmotic stress. To measure the cell volume, we manually traced the outline of the cell in the phase-contrast image, measured the mean intensity in the corresponding region in the fluorescence image, and subtracted this value from the fluorescence intensity of the background. The resulting intensity difference was converted to the mean height of the cell using the calibration described above and multiplied by the cell area to obtain the cell volume. Note that the accuracy of the tracing of the cell outline does not have a strong influence on the determination of the volume. Indeed, taking a larger area than the cell would result in a lower intensity difference between the cell and the background; multiplying this difference by a larger area is expected to give in principle the same value of the volume. In noisy images, however, taking too large area may increase the error. To facilitate precise tracing of the cell outline, we have recently developed an automatic level set-based segmentation algorithm.[35]

A typical cell volume response to osmotic stress is shown in Fig. 4A and the corresponding phase-contrast and fluorescence images are presented in panels B–E. The volume was nearly constant in isotonic medium, but started to increase quickly after the transition to a hypotonic solution. After swelling from an initial volume of 330 μm^3 to a maximum of 650 μm^3 during the

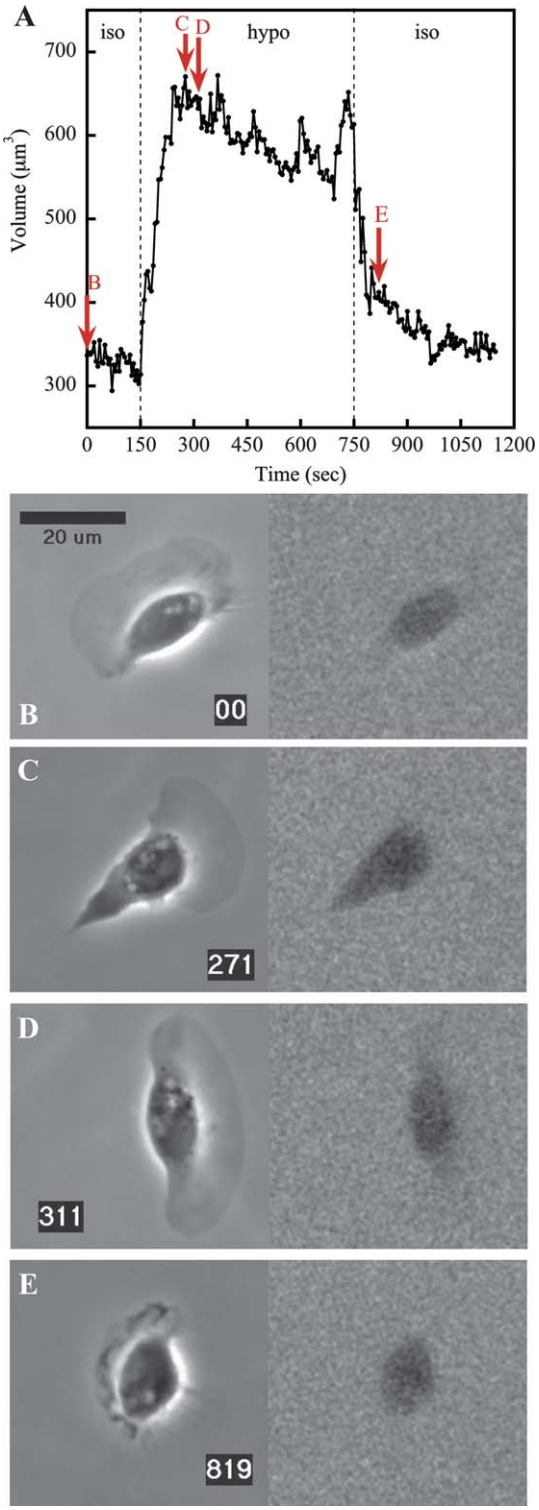

Fig. 4 Response of a single migrating cell to osmotic stress. (A) Dynamics of volume changes. The vertical dashed lines indicate the times when the osmotic transitions were applied. (B), (C), (D), and (E) show phase-contrast (left) and fluorescence (right) images of the cell at the time points indicated by the red arrows in (A). Images were taken with a 40× lens. Time is indicated in seconds. Bar: 20 μm.

first 100 seconds after the transition, the cell volume slowly decreased to a final value of 550 μm³. Then, a hyper-osmotic transition was applied at 750 seconds by injecting isotonic solution, which induced rapid shrinkage of the cell to a volume of 400 μm³. During the last 400 seconds of the experiment, the volume slowly decreased to a value of 340 μm³, similar to the initial volume. We measured the relative volume increase in several cells. On average, the cell volume increased by a factor of 2.1 ± 0.3 ($N = 7$ cells) upon hypotonic treatment and decreased back to 1.7 ± 0.2 ($N = 7$ cells) of the initial volume after 10 min of adaptation in hypotonic solution. These observations are in contrast to a previous study of osmotic response in Xenopus keratocytes as measured by interference reflection microscopy.[20] In this study, the authors used a rather complex and indirect method of counting interference fringes and measured a much lower degree of swelling than what we observed in our experiments. These authors explained the low swelling by contractions of the actomyosin system that counteract the volume response to osmotic stress. In contrast, our carefully validated measurements using the fluorescence displacement method indicate that the initial degree of swelling is nearly equal to the degree of dilution of the medium. This suggests an initial passive response of the cell to the osmotic shock, which may be followed by active adaptive responses.

Concomitant with volume changes, significant perturbations of the cell shape were observed soon after the osmotic transitions (Fig. 4C and E), but the cell rapidly recovered its regular shape (Fig. 4D). Even without precise quantification of volume changes, simple visual examination of the intensity of the cell shadow in the fluorescence images gives an idea about the state of the cell: normal (Fig. 4B), swollen (Fig. 4C and D), or shrunk (Fig. 4E). However, the fine cell structures, such as the lamellipodium, are not reliably detected in the images obtained in a thick microfluidic channel with a low-power objective (40×).

The sensitivity of our method with respect to the detection of thin cell structures depends on the ability to measure small differences in fluorescence intensity over a significant background. Thus, the sensitivity is defined essentially by the dynamic range and noise of the image sensor. We estimate that the smallest intensity difference between small image areas that we could measure with our setup is approximately ten units of the intensity readout. Indeed, the standard deviation of the pixel values in the uniform image areas was measured to be approximately 25. Applying Student's *t*-test, one could see that a few hundred pixel-measurements are sufficient to detect a mean intensity difference of 10 over a standard deviation of 25 with 99.9% certainty. In our setup, 200 pixels correspond to a cell area of approximately 1 micrometre square or approximately 6 micrometres square with 100× and 40× lenses, respectively. When using a thick observation chamber, the exposure time or the dye concentration has to be reduced in order to keep the background fluorescent intensity within the dynamic range of the camera. This effectively reduces the intensity difference that can be measured for a given height difference, while the image noise does not change. In particular, using a 14-bit camera and a thick chamber, we observed that the intensity difference that could be measured per micrometre of height is in the order of 50 readout units (see calibration curves in Fig. 2 and note that the values obtained in a thick chamber were multiplied by 5 to compensate for the dye dilution). Thus, the lamellipodium height of about 200 nm would result in an intensity difference of 10 units, which is at the limit of detection. Increasing the dynamic range of the detector or decreasing the chamber thickness is expected to increase the sensitivity. Indeed, using a thinner chamber allows increasing exposure time and measuring intensity differences of a few hundred readout units per micrometre of height. Thus, we expect to detect features of a few tens of nanometres thickness, provided that the projection area of these features is in the order of a few micrometres square.

To test the sensitivity of the method in a thin chamber, we imaged a cell during swelling in the custom chamber with a high-power objective (100×). Fig. 5 shows the phase-contrast and fluorescence images of the cell in normal (A) and swollen (B) states. The corresponding height profiles clearly revealed the shape of the lamellipodium (Fig. 5C, inset). Swelling response involved an increase in the lamellipodium height, while the height of the cell body did not change significantly (swelling also resulted in the cell area increase as evident from the images). Moreover, the fluorescence image of the swollen cell (Fig. 5B) revealed inhomogeneity in the lamellipodium region with swelling mostly localized in the central part. Thus, our measurements demonstrate that sub-micrometre changes in the

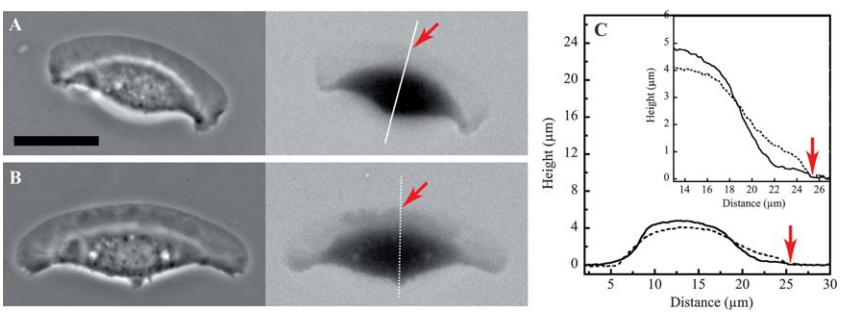

Fig. 5 Changes in the cell morphology and height profile under hypoosmotic stress. We show phase-contrast (left) and the corresponding fluorescence (right) images of a migrating cell in isotonic medium (A) and 2.5 min after transition to a hypotonic medium (B). (C) Height profiles along the solid white line shown in (A) (solid line) and the dotted white line shown in (B) (dotted line). The inset in (C) shows the details of the front part of the cell in extended scale of height. Red arrows indicate the position of the cell's leading edge in the fluorescence images and the intensity profiles. Images were taken with a 100× lens. Bar: 20 μm.

cell height in the course of a dynamic cellular response can be reliably detected with conventional wide-field fluorescence microscopy. Application of the fluorescence displacement method in future studies of cell volume dynamics will help us understand the detailed kinetics and morphological features of cell responses to osmotic changes.

Conclusions

We have proposed a new and simple method, termed fluorescence displacement technique, to dynamically measure the height and volume of migrating cells. The method is based on measuring the decrease in fluorescence intensity when a fluorescent solution is displaced by a non-fluorescent transparent object, *e.g.* a cell, in a chamber of uniform height. In contrast to previous studies implying a similar negative staining principle, we utilize conventional wide-field fluorescence microscopy. We showed that the decrease in fluorescence intensity is proportional to the height of the displacing object and that the measurements do not depend on the position of the focal plane in a wide interval. The calibration sample made of Pyrex etched at several defined depths permitted relating fluorescence intensity to height and measuring height profiles and volumes of migrating cells. These measurements were validated by comparison with AFM results.

The fluorescence displacement technique is extremely simple and does not require specialized equipment. A conventional epifluorescence microscope is sufficient and the setup is compatible with other modes of microscopy, such as fluorescence of intracellular markers (in other colour channels) and phase-contrast microscopy. Thanks to the fast image acquisition, the technique is well suited to image rapidly migrating cells. From a biological point of view, it allows extracting supplementary parameters (*i.e.*, volume and height profile), which are complementary to the ones measured in other modes of microscopy (*i.e.*, velocity, shape, area, and distribution of intracellular markers). Indeed, we were able to observe concomitant changes in the cell shape, volume, and vertical profile during the response to osmotic stress. Future work may uncover intrinsic relationships between cell shape, velocity, height, and volume, providing a better understanding of the cell migration mechanism.

Acknowledgements

This work was supported by Swiss National Science Foundation grant 31003A-135661 for A.B.V and by an iPhD fellowship from the Swiss SystemsX.ch initiative, evaluated by the Swiss National Science Foundation, to A.B.V. and I.F.S. The authors also thank Josiane Smith for the culture and preparation of the fibroblasts.

Notes and references

1 F. Lang, G. L. Busch, M. Ritter, H. Völkl, S. Waldegger, E. Gulbins and D. Häussinger, *Physiol. Rev.*, 1998, **78**, 247–306.
2 E. K. Hoffmann, I. H. Lambert and S. F. Pedersen, *Physiol. Rev.*, 2009, **89**, 193–277.
3 S. Saadoun, M. C. Papadopoulos, M. Hara-Chikuma and A. S. Verkman, *Nature*, 2005, **434**, 786–792.
4 S. Rosengren, P. M. Henson and G. S. Worthen, *Am. J. Physiol. Cell Physiol.*, 1994, **267**, C1623–C1632.
5 M. Ritter, P. Schratzberger, H. Rossmann, E. Woll, K. Seiler, U. Seidler, N. Reinisch, C. M. Kahler, H. Zwierzina, H. J. Lang, F. Lang, M. Paulmichl and C. J. Wiedermann, *Br. J. Pharmacol.*, 1998, **124**, 627–638.
6 A. Schwab, B. Schuricht, P. Seeger, J. Reinhardt and P. C. Dartsch, *Pfluegers Arch.–Eur. J. Physiol.*, 1999, **438**, 330–337.
7 D. Raucher and M. P. Sheetz, *J. Cell Biol.*, 2000, **148**, 127–136.
8 C. I. Lacayo, Z. Pincus, M. M. VanDuijn, C. A. Wilson, D. A. Fletcher, F. B. Gertler, A. Mogilner and J. A. Theriot, *PLoS Biol.*, 2007, **5**, e233.
9 K. Keren, Z. Pincus, G. M. Allen, E. L. Barnhart, G. Marriott, A. Mogilner and J. A. Theriot, *Nature*, 2008, **453**, 475–480.
10 L. Ji, J. Lim and G. Danuser, *Nat. Cell Biol.*, 2008, **10**, 1393–1400.
11 A. Mogilner and B. Rubinstein, *J. Phys.: Condens. Matter*, 2010, **22**, 194118.
12 J. Satulovsky, R. Lui and Y. L. Wang, *Biophys. J.*, 2008, **94**, 3671–3683.
13 K. Keren, P. T. Yam, A. Kinkhabwala, A. Mogilner and J. A. Theriot, *Nat. Cell Biol.*, 2009, **11**, 1219–1225.
14 A. F. Brown and G. A. Dunn, *J. Cell Sci.*, 1989, **92**, 379–389.
15 D. Zicha, I. M. Dobbie, M. R. Holt, J. Monypenny, D. Y. H. Soong, C. Gray and G. A. Dunn, *Science*, 2003, **300**, 142–145.
16 E. C. Gregg and K. D. Steidley, *Biophys. J.*, 1965, **5**, 393–405.
17 S. Z. Hua and T. Pennell, *Lab Chip*, 2009, **9**, 251–256.
18 D. A. Hill, S. Chiosea, S. Jamaluddin, K. Roy, A. H. Fischer, D. D. Boyd, J. A. Nickerson and A. N. Imbalzano, *J. Cell Sci.*, 2004, **117**, 5847–5854.
19 T. Nakahari and Y. Imai, *J. Membr. Biol.*, 1998, **161**, 287–296.
20 R. Strohmeier and J. Bereiter-Hahn, *J. Cell Sci.*, 1987, **88**, 631–640.
21 F. Boudreault and R. Grygorczyk, *J. Microsc.*, 2004, **215**, 302–312.
22 S. Schneider, P. Pagel, C. Rotsch, T. Danker, H. Oberleithner, M. Radmacher and A. Schwab, *Pfluegers Arch.–Eur. J. Physiol.*, 2000, **439**, 297–303.
23 Y. E. Korchev, J. Gorelik, M. J. Lab, E. V. Sviderskaya, C. L. Johnston, C. R. Coombes, I. Vodyanoy and C. R. W. Edwards, *Biophys. J.*, 2000, **78**, 451–457.
24 M. Zelenina and H. Brismar, *Eur. Biophys. J.*, 2000, **29**, 165–171.
25 W. E. Crowe and N. K. Wills, *Pfluegers Arch.–Eur. J. Physiol.*, 1991, **419**, 349–357.
26 M. A. Model, A. K. Khitrin and J. L. Blank, *J. Microsc.*, 2008, **231**, 156–167.
27 J. L. Gregg, K. M. McGuire, D. C. Focht and M. A. Model, *Pfluegers Arch.–Eur. J. Physiol.*, 2010, **460**, 1097–1104.
28 M. Pelts, S. M. Pandya, C. J. Oh and M. A. Model, *BioTechniques*, 2011, **50**, 389–396.
29 M. S. Droste, S. S. Biel, L. Terstegen, K. P. Wittern, H. Wenck and R. Wepf, *J. Biomed. Opt.*, 2005, **10**, 064017.
30 K. I. Anderson, Y. L. Wang and J. V. Small, *J. Cell Biol.*, 1996, **134**, 1209–1218.
31 J. Lee, A. Ishihara and K. Jacobson, *Symp. Soc. Exp. Biol.*, 1993, **47**, 73–89.
32 V. M. Laurent, S. Kasas, A. Yersin, T. E. Schäffer, S. Catsicas, G. Dietler, A. B. Verkhovsky and J.-J. Meister, *Biophys. J.*, 2005, **89**, 667–675.
33 C. A. Brunner, A. Ehrlicher, B. Kohlstrunk, D. Knebel, J. A. Käs and M. Goegler, *Eur. Biophys. J.*, 2006, **35**, 713–719.
34 T. M. Svitkina, A. B. Verkhovsky, K. M. McQuade and G. G. Borisy, *J. Cell Biol.*, 1997, **139**, 397–415.
35 M. E. Ambühl, C. Brepsant, J.-J. Meister, A. B. Verkhovsky and I. F. Sbalzarini, *J. Microsc.*, 2011, in press.